Journal of Hazardous Materials, 16 (1987) 43–74
Elsevier Science Publishers B.V., Amsterdam — Printed in The Netherlands

ANALYSIS OF METEOROLOGICAL DATA FOR THE THORNEY ISLAND PHASE I TRIALS

J.S. PUTTOCK

Shell Research Ltd., Thornton Research Centre, P.O. Box 1, Chester CH1 3SH (Great Britain)

(Received February 3, 1987; accepted May 21, 1987)

Summary

The validation of dense-gas dispersion models against field data requires not only examination of gas concentration data, but also accurate determination of input parameters. A full analysis of meteorological data from Phase I of the Thorney Island dense-gas dispersion trials has been performed. Parameters such as mean wind speed and ambient temperature were easy to obtain, but determination of atmospheric stability and surface roughness was less straightforward. The data from ten sonic anemometers were used, after removal of faulty signals. It was found that the use of long averaging periods and high-pass filtering was necessary to obtain good estimates of the vertical fluxes of heat and momentum.

The determination of atmospheric stability from vertical heat flux showed a few discrepancies with an assessment based on simple weather observations. Values of the surface-roughness length, derived from the momentum flux, had a range of two orders of magnitude. The high values in some trials appear to have been caused by buildings and trees upwind, and the low values for other wind directions may be due to the sea upwind.

This study has demonstrated that atmospheric conditions are frequently transitory, and has underlined the care that is required in taking meteorological measurements when using field trials for the validation of dispersion models.

1. Introduction

The experiments in Phase I of the Thorney Island Heavy Gas Dispersion Trials concerned dispersion over an unobstructed flat surface. The site has been described by Davies and Singh [1]. Sixteen releases were made of about 2000 m^3 of a freon/nitrogen mixture at a density normally about twice that of air. The gas was initially held in a "tent" 14 m high and 14 m diameter, whose sides were dropped rapidly to release the gas. Gas concentrations were measured at about forty masts each holding four or more gas sensors. The data from these can be compared with predictions from dense-gas dispersion models.

Model validation, however, requires not only examination of the gas concentration data, but also accurate determination of input parameters. For this reason a careful analysis of the meteorological data is needed and, although

values for the mean wind speed and ambient temperature are easy to obtain, the determination of atmospheric stability and surface roughness is less straightforward.

It is necessary to obtain values for the surface roughness and atmospheric stability since both can have an important effect on dispersion. The surface roughness is a key parameter of the surface boundary layer. It determines friction velocity u_* and hence turbulence levels. Thus it has a significant effect on mixing. Local values can be determined from the nature of the surface, but the effective value may be influenced by upwind terrain.* Atmospheric stability also affects turbulence levels. In a stable atmosphere (potential temperature gradient, $dT/dz > 0$) turbulence is suppressed and mixing reduced. With dense gases this principally affects far-field disperion.

Analysis of the meteorological data has been performed for fifteen Phase I trials (excluding the early nitrogen release, Trial 4). Particular emphasis has been placed on the data from the ten sonic anemometers located at various points in the measurement array. Cross-correlations of the vertical velocity with the horizontal velocity and with the "temperature" measurements give values for shear stress and density flux. From these, the effective surface roughness and atmospheric stability are obtained directly.

2. Sensor status and corrections

2.1 Sonic anemometer status

Johnson [3] has described the sensors used in the trials, and their mounting. The main meteorological station was a mast 30 m high located 150 m upwind of the spill point. Kaijo Denki model DAT-300 sonic anemometers were used for turbulence measurements. Two of these were mounted on the main meteorological mast, and eight others elsewhere in the array so that turbulence levels in the gas clouds might be measured. These could be used for the determination of ambient conditions when they were not covered by the gas cloud. For most of the trials, half of the anemometers were at 2 m above the surface, with the others at higher levels up to 20 m.

The DAT-300 anemometer determines the vertical component of velocity, and two horizontal components at 120° to one another, which can be resolved to orthogonal components. The sound speed along the vertical path is also used

*It may be argued that roughness length in a crude single parameter compared with the fairly comprehensive ambient turbulence measurements available during these experiments. However, roughness length is the parameter used by most dispersion models to characterise the surface, since nothing more is typically available. Furthermore, in a very dense cloud the turbulence will be considerably modified; the ambient turbulence may have very little relevance there compared with that generated by the interaction of the dense flow with the local surface. This is discussed by Puttock [2].

to determine air temperature approximately, ignoring the effect of humidity fluctuations (see Puttock and Colenbrander [4]).

The instrument has a resolution of 0.005 m/s and accuracy of 1%. For temperature the range is $\pm 5\,^{\circ}$C about a manually set mid-point, with a resolution of $0.025\,^{\circ}$C. Digitised data were collected at 20 Hz.

Since a variety of faults can arise with the sonic anemometers, some of which are not immediately obvious from the data, it is necessary to examine the signals carefully in order to exclude bad data. The status of each anemometer channel was determined by examination of the full-length signal, together with more detailed investigation of sensors which produced anomalous values of σ_u/u_* or σ_w/u_*. The anomalous values were not rejected, however, unless the detailed examination revealed evidence of sensor faults.

In some cases no signal, or a contant output, was produced. A fairly common fault in these sensors is evidenced by sudden shifts of level in output. When the shifts to the second level are only brief, the sensor shows a series of spikes. In mild cases it can be difficult to distinguish these faults from genuine changes in the wind, but on close examination the erroneous jumps in signal are found to occur between two consecutive data points, only 0.05 s apart. The genuine changes take longer. Data from all the faulty channels have been excluded from further analysis. These faulty signals comprise some 8% of the sonic anemometer data collected. (Details are available from the author.)

Finally, since the presence of gas may change the flow, as well as affecting the temperature channels, data from the periods when gas was present at a location have been excluded from our analysis. This exclusion has been applied to all levels even when gas was only detected at one level.

2.2 Angular dependence of measured wind speed

The sonic anemometer is designed to make measurements along its axis, and it is intended that in normal use it should be turned to face, roughly, the mean wind direction. At Thorney Island it was not possible to make changes in the alignment of the anemometers before each test, and so they were permanently aligned with the axis of the sensor array. It is generally accepted that there are problems with data when the wind direction is more than 45° from the axis since the transducers and the arms on which they are mounted obstruct the flow. Tests with the Kaijo Denki anemometer in a steady wind in a wind tunnel (Fig. 1) show a 5% change in the indicated wind speed at only 30° from the axis. It was intended that the trials would be performed with the wind direction within about 30° of the array axis. However, in practise, the mean wind direction was in this range for less than half the Phase I tests.

The sonic anemometer measurements in the Thorney Island data are corrected for this effect in the compilation of the data tapes by BMT, using wind tunnel measurements similar to those in Fig. 1. The correction is not exact

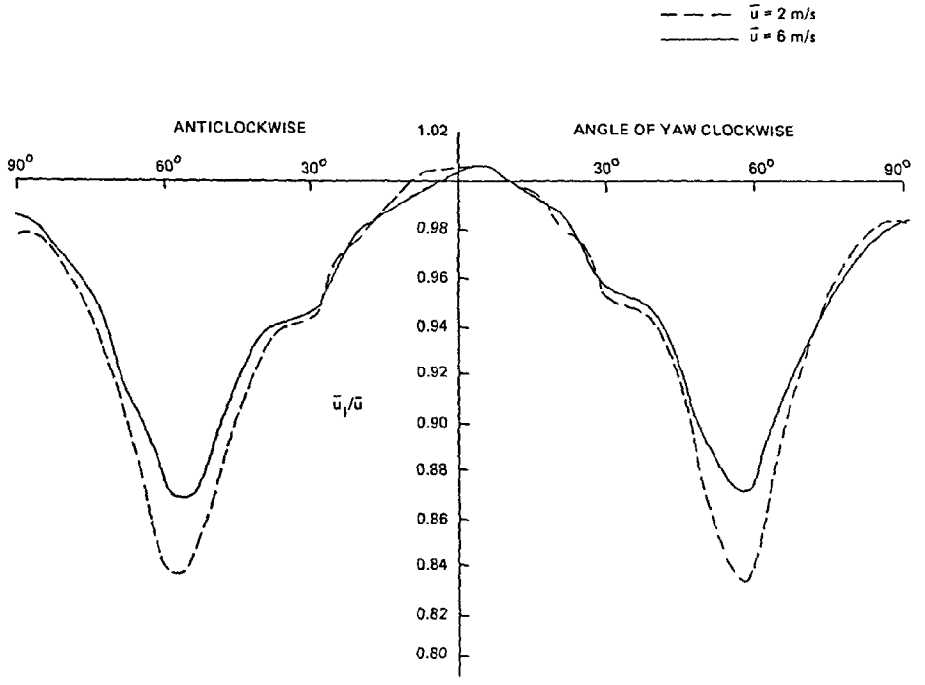

Fig. 1. Variation of indicated wind speed $\bar{u}_i$ with angle of yaw.

since the response in a highly turbulent flow would not be the same as in the steady flow in the wind tunnel.

As it was thought that the correction procedure would yield a more accurate value for the horizontal component of wind speed, rather than for the two horizontal components of wind velocity separately, this quantity, denoted here by 'u', was used in all further analysis. This choice also avoids the difficulty inherent in using the longitudinal component of wind velocity, which is dependent on the mean wind direction and so is dependent on the averaging period used.

The mean wind speeds obtained from the sonic anemometers on the meteorological mast were compared with those from the cup anemometers at the same locations. It was found that, with the wind aligned with the axis, the ratio of sonic to cup windspeed was about 0.94. This is consistent with a 5 to 10% overspeeding of the anemometers.* At 2 m, the ratio remained around 0.94 for other wind directions (with the exception of two anomalous values around 1.2,

*Since they respond more rapidly to velocity increases than to decreases, cup anemometers give too high a value for mean velocity in a turbulent flow. Wyngaard [5] cites data showing up to 10% overspeeding in the atmosphere; Högström [6] found 5%.

which are unexplained). However, at 10 m for increasing wind angle θ (measured from the array axis), the ratio was found to increase, peaking near $\theta = 50°$ at 0.99. This is still satisfactory. From an examination of cup and sonic anemometer readings from all locations and heights it was concluded that the main reason for the variation with wind direction was not that the sonic anemometer correction was inappropriate, but that obstructions on the mast affected the 10 m cup anemometer for large wind angles.

2.3 Tilt, flow-distortion and heat-flux corrections

A slight tilt of the sonic anemometer, or distortion of the flow by nearby obstacles, can result in contamination of the measured vertical velocity by a small part of the longitudinal velocity fluctuations. Puttock and Colenbrander [4] have suggested a correction which approximates the corrections for both these effects derived by Dyer [7,9] and Wyngaard [8]:

$$\overline{u'w'} = \overline{u'_m w'_m} - \frac{\bar{w}_m}{\bar{u}_m}\overline{u'^2_m}$$

where the subscript m denotes measured values. This correction can be substantial, but is easily calculated from the measured data and has been applied in the data analysis. In the few cases with a particularly large $\bar{w}_m$ [$(\bar{w}_m/\bar{u}_m) > 0.05$], the data have been exluded from further analysis.

It is possible for $\bar{w}$ to be genuinely different from zero, because of the finite length of the averaging period. It could be, therefore, that this correction is being applied inappropriately. To test its utility, the consistency of values of $\overline{u'w'}$ computed from the various sonic anemometers was compared before and after correction. To do this the weighted standard deviation, as defined in Section 4, was computed. The results are listed in the first part of Table 1. Whatever the genuine variability of measurements of shear stress at various locations for the periods used, addition of random errors would be expected to increase the scatter, and their removal to decrease it. In fact, the correction does produce a significant improvement on average, and so its use has been retained.

The correction term $-2\,(\bar{T}\,\bar{u}/\overline{C^2})\,\overline{u'w'}$ for the measured "heat flux" $\overline{w'_m\,T'_m}$ has also been applied. Schotanus et al. [10] have shown that this correction is necessary for reliable flux measurements.

No attempt has been made to correct for the effect of humidity flux since, as discussed by Puttock and Colenbrander [4], the result of ignoring the humidity effect is to leave $\overline{w'_m T'_m}$ approximately proportional to the buoyancy flux, which has more direct significance in the boundary-layer dynamics than heat flux alone.

2.4 The resolution of the temperature channel data

There is a potential problem associated with the sonic anemometer temperature channels, owing to the way the signals from these channels were digi-

TABLE 1

Weighted standard deviations of measurements of momentum flux ($-\overline{u'w'}=u_*^2$), before and after tilt correction and then with high-pass filter applied

Trial	Without tilt correction	With tilt correction	With tilt correction and filtered
5	0.659	0.728	0.783
6	0.369	0.347	0.161
7	0.249	0.164	0.232
8	0.759	0.526	0.444
9	0.311	0.440	0.407
10	0.550	0.467	0.219
11	0.265	0.245	0.092
12	0.638	0.581	0.523
13	0.221	0.140	0.129
14	0.629	0.480	0.542
15	0.415	0.323	0.259
16	0.421	0.259	0.251
17	0.309	0.259	0.102
18	0.307	0.210	0.260
19	0.336	0.251	0.244
Mean[a]	0.370	0.286	0.227

[a]The mean excludes Trials 5, 8, 9 and 12, where the boundary layer appears to have been far from a constant-flux condition.

tised. The anemometer output was zero for 0°C rising to 0.8 V for 40°C. This output was applied, without amplification, to a twelve-bit analogue-to-digital converter with an input range of ±10 V. Thus the A to D resolution is approximately 5 mV (20 V/4096) corresponding to about 0.25°C temperature resolution, an order of magnitude worse than the capability of the instrument.

The consequence of this is that, if the temperature fluctuations were very small the digitised signal could be constant, or alternatively amplified to steps of 0.25°C.

In order to investigate the practical consequences of poor temperature resolution on "heat flux" $\overline{w'T'}$, we have used the signals from the high-speed thermometers available in Trials 15–19. The signals, which in fact had good resolution, were artificially reduced to steps of size ΔT, where ΔT could be varied. The cross-correlation $\overline{w'T'}$ was calculated using the degraded signals. This was normalised with $\overline{w'T'}$ from the original temperature signals, and plotted against $\Delta T/\sigma_T$, where σ_T is the standard deviation of temperature.

The results show that for $\Delta T/\sigma_T$ up to a value of 1, there is very little effect of coarsening resolution. Up to $\Delta T/\sigma_T=2$, $\overline{w'T'}$ is within 10% of the correct value. Beyond this, the correlation drops off rapidly to zero at $\Delta T/\sigma_T=6$.

It thus appears that in Trials 6, 7 and 11 the errors in individual values of $\overline{w'T'}$, due to this effect, could be approaching 10%. For the remaining trials the effect would be very small.

3. High-pass filtering

It is generally accepted that trends and periodicities in velocity data, which result in the signals being statistically non-stationary, can have a serious effect on the spectra of turbulent fluxes in the atmosphere [11]. But it is not clear from the literature whether their removal is essential in the determination of the integral properties, e.g. $\overline{u'w'}$.

There are various ways of dealing with such data. McBean and Elliott [12] simply removed linear trends. But a more comprehensive approach is to apply some kind of high-pass filtering. The simplest method is the continuous subtraction of a moving average, as suggested by Kaimal et al. [11]. Van Haren [13] has shown there is little practical difference between this approach and applying a filter with a sharp frequency cut-off.

If the moving-average method is used, an averaging period has to be chosen. McBean [14] used a filter with a cut-off frequency n given by $f \equiv nz/\bar{u} = 0.003$. However, this figure seems to have been derived from measurements on one height. In a study of a sample of Maplin Sands data [13], surprisingly no significant effect of windspeed or height on the necessary averaging period was found.

In order to investigate the effect of high pass filtering, a number of tests were performed with Thorney Island data. Four trials were chosen, covering a range of wind speeds and stabilities, and two sonic anemometers used from each (normally at 2 m and 15 m on the same mast). Moving averages with a range of averaging periods, up to 400 s, were subtracted from the basic u, w and T signals. Then $\overline{u'w'}$, $\overline{w'T'}$, σ_u, σ_w and σ_T were computed from these filtered signals and also from the original, unfiltered, data. The same data period, about 500 s long, was used for the final averaging in all cases for a particular trial; thus 900 s of initital data was required for the longest moving-average period to accomodate the run-up and run-down time of the moving average.

Results from Trial 16 are shown in Fig. 2. This particularly well-behaved dataset shows the rise to a plateau in the values when the moving-average period is long enough; it also illustrates the finding that very often the values obtained without filtering are the same as those with filtering of sufficiently long period. However, there were examples where this was not the case. Figure

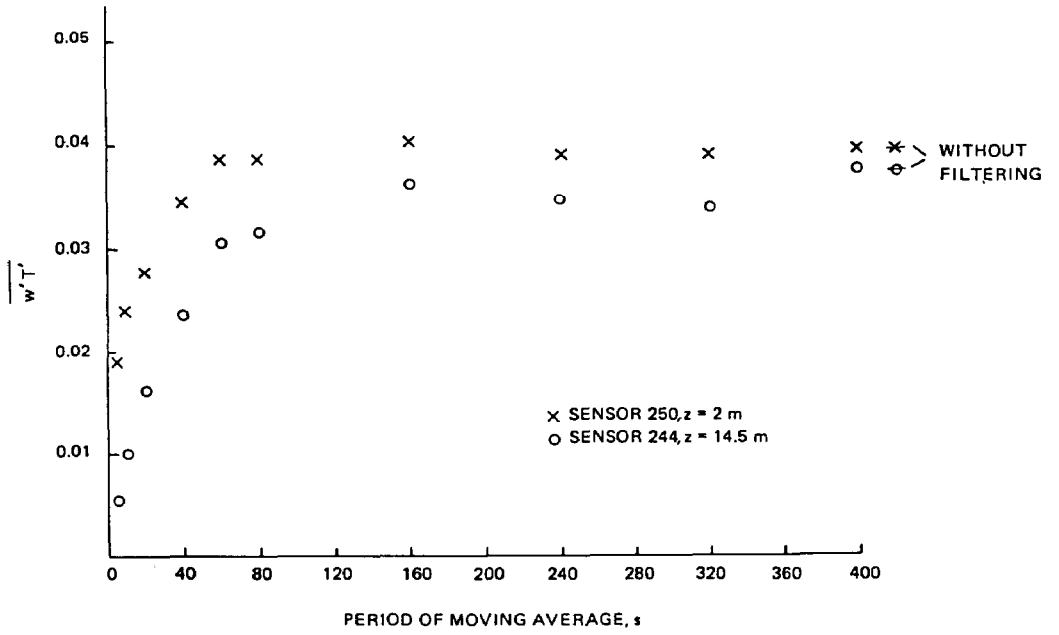

Fig. 2. The effect of varying the moving-average period used in the high pass filter on $\overline{w'T'}$, Trial 16.

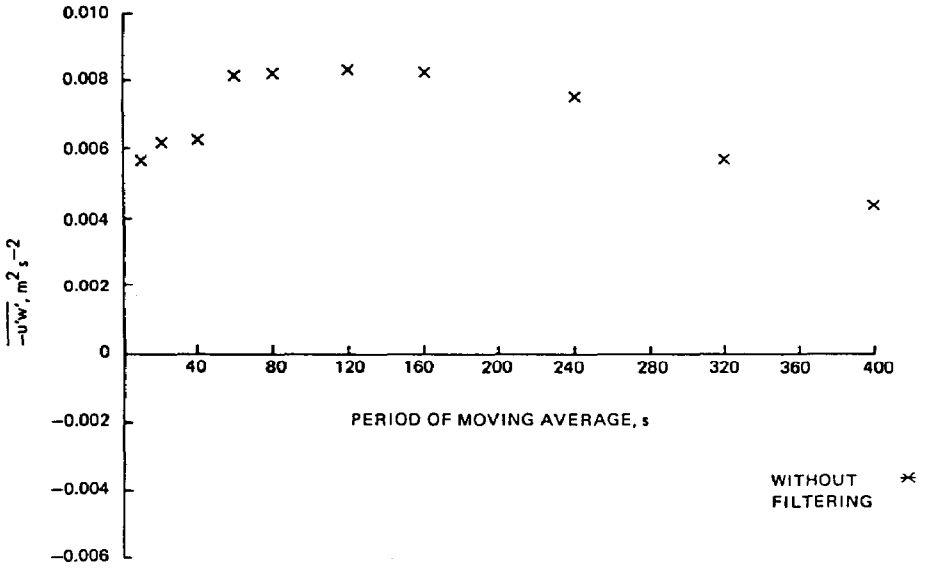

Fig. 3. The effect of varying the moving-average period in the high pass filter on $\overline{u'w'}$, Trial 12. Without the filter $\overline{u'w'}$ has the opposite sign.

3 shows an extreme case where, with filtering, a well-defined plateau is found for $\overline{u'w'}$, but without filtering $\overline{u'w'}$ is grossly different, in fact positive.*

The moving-average period for which the various correlations reached 80% of their plateau values were read from plots such as those in Fig. 2. It would appear that twice this period generally needs to be used to give a good estimate of the plateau value. From this study of four trials, it was concluded that a fixed moving-average period of 120 s should be used; this would be expected to give good results in all cases except the high sensors in low-wind, unstable trials.

All the analysis has been performed both with and without the high-pass filter applied. One method of assessing the effect of filtering is again to examine the consistency of the measurement of shear stress. The normalised weighted standard deviations of the measurements of $-\overline{u'w'}$ are shown in Table 1. There are a number of trials where filtering produces a large improvement. These are presumably trials where low-frequency variations are significant. Many others show a small improvement with filtering. However, there are a few trials where the standard deviation is significantly increased by filtering. For these, perhaps, 120 s is not long enough.

Since it appears that the chosen high-pass filter may have been inappropriate for these latter trials, it was decided to use the standard deviations to decide whether to use filtered or unfiltered data in the final plots in section 6. Thus unfiltered data were used for Trials 5, 7, 14 and 18.

4. Weighting

In all the trials some of the sonic anemometers were affected by the presence of gas for part of the data period. This reduces the interval from which useful ambient data can be obtained from these sensors. The effect of using small averaging times for these sensors is that the estimates of $\overline{u'w'}$, for example, are more widely scattered; this would be expected, assuming that the standard deviation is proportional to $t_a^{-1/2}$, where t_a is the averaging time. It is correct to include these observations in the calculation of the overall average of, say, $\overline{u'w'}$ for the trial, provided a weighting proportional to t_a is used.

In addition to the effect of averaging time, the height of the sensor above the surface also affects the standard deviation of the measurements since the integral time scale of the turbulence is roughly proportional to the height z. Puttock and Colenbrander [4] derive an estimate of the relative error:

*In our initial analysis, as a result of a misunderstanding, the direction-dependent correction (see Section 2.2) was applied to the sonic anemometer data that had already been corrected by BMT. When the double correction was pointed out, all analysis was repeated, except for the investigations described in this section, whose conclusions would be unchanged if all data points for a particular trial were multiplied by a (roughly) constant factor. Thus the $\overline{u'w'}$ values plotted in Figure 3 are consistently about 10% too high.

$$\epsilon \simeq \left(\frac{20\,z}{\bar{u}\;t_a}\right)^{1/2} \tag{4.1}$$

Since the expected z-dependence did not appear for the necessary moving-average periods (Section 3), we have not relied on the theoretical predictions here, but have investigated this error practically. In each trials the standard deviation of measurements of $\overline{u'w'}$ at 2 m has been determined, and similarly for measurements at 15 m $\pm$ 5 m. Data were only used where there were two operational sensors on the same mast, with usable data lengths of greater than 360 s. The results were then averaged over all trials (excluding those which did not produced a value, having no more than one operational pair of sensors at the specified heights).

The resulting average values of $\bar{u}^{1/2}\,\epsilon$ were 0.22 and 0.66 $m^{1/2}\,s^{-1/2}$ at 2 m and 15 m respectively (using filtered data). These values compare remarkably well with the predictions of eqn. (4.1) which, taking a representative data length t_a as 600 s, gives 0.26 and 0.71 $m^{1/2}\,s^{-1/2}$.

These findings confirm the appropriateness of using a weighting proportional to t_a/z. Thus the weighted mean of a quantity x will be calculated as:

$$\bar{x} = \frac{\sum w_i x_i}{\sum w_i} \qquad w_i = \frac{t_i}{z_i}$$

where z_i is the measurement of the quantity by sensor i, t_i is the data length used from sensor i, and z_i is the height above the surface of sensor i.

In some circumstances, it will be useful also to have a measure of the scatter of observations of the quantity. In such cases we can define a weighted standard deviation as:

$$\left(\frac{\sum w_i\;(x_i - \bar{x})^2}{\sum w_i}\right)^{1/2}$$

There is some doubt about whether this is an appropriate statistic for comparing different trials, where the weights may differ; but it can certainly be useful, as described in Sections 2 and 3, in comparing methods of treating the same data.

5. Data reduction

5.1 Basic data from sonic anemometers

For each sonic anemometer, $\bar{u}$, σ_u ($\equiv (\overline{u'^2})^{1/2}$), $\bar{w}$, σ_w, $\bar{T}$ and σ_T have been computed. The mean values presented are taken from unfiltered data in all cases, since for the filtered data the means are approximately zero.

σ_u/u_*, σ_w/u_* and $\sigma_T T_*$ have been computed for comparison with findings at other sites. u_* and T_* are defined by:

$$u_*^2 = -\overline{u'w'}$$
$$u_* T_* = -\overline{w'T'}$$

5.2 Determination of the Monin–Obukhov length L *and the Kazanski–Monin stability parameter,* μ

The similarity theory of Monin and Obukhov [15] for the stratified atmospheric boundary layer is well supported by observation. In this theory a boundary layer with constant fluxes of heat and momentum is parameterised by z/L. A good estimate of the Monin–Obukhov length L can be obtained from [4]:

$$L = -\frac{u_*^3 \bar{T}}{k_v g \overline{w'T'}_c}$$

where k_v is the von Karman constant, and g gravitational acceleration. This is used in the analysis below.

An alternative, dimensionless, parameter describing the stability of the boundary layer is the Kazanski–Monin stability parameter [16,17]:

$$\mu = \frac{k_v u_*}{f_c L}$$

where f_c is the Coriolis parameter (1.12×10^{-4} s^{-1} at latitude 51°N).

5.3 Determination of the roughness length

The roughness length, z_0, can be determined from momentum flux and velocity profile measurement in a neutral boundary layer, using the logarithmic profile relation:

$$\bar{u}(z) = \frac{u_*}{k_v} \ln (z/z_0) \tag{5.1}$$

where $\bar{u}$ is mean velocity, k_v the von Karman constant, and $u_* = (-\tau/\rho)^{1/2} = (\overline{u'w'})^{1/2}$ is the friction velocity. However, confining consideration to exactly neutral conditions would considerably restrict the data available for analysis, and so it is necessary to take account of stratification. Standard expressions for the stratified boundary layer are [18]:

$$\frac{\partial \bar{u}}{\partial z} = \frac{u_*}{k_v z} \phi_m (z/L) \tag{5.2}$$

$$\frac{\partial \bar{T}}{\partial z} = \frac{T}{k_v z} \phi_h (z/L) \tag{5.3}$$

with, for unstable stratification ($z/L < 0$):

$$\phi_m = (1 - \alpha z/L)^{-1/4} \tag{5.4}$$

$$\phi_h = A\ (1-\gamma\ z/L)^{-1/2} \tag{5.5}$$

and, for stable stratification ($z/L<0$):

$$\phi_m = 1+\beta_1\ z/L \tag{5.6}$$

$$\phi_h = A+\beta_2\ z/L \tag{5.7}$$

For the constants, we follow Wieringa's [19] re-analysis of Kansas data:*

$$\begin{array}{cccccccc} k_v & = & 0.41 & \alpha & = & 22 & \beta_1 & = & 6.9 \\ A & = & 1 & \gamma & = & 13 & \beta_2 & = & 9.2 \end{array} \tag{5.8}$$

The temperature gradient relations (involving ϕ_h) have been included here for completeness and will be used in Section 6.5. Restricting attention to ϕ_m, it can be shown that eqns. (5.2, 5.4 and 5.6) integrate to:

$$\bar{u}\ (z) = \frac{u_*}{k_v}\ (\ln \frac{z}{z_0} - \phi_m) \tag{5.9}$$

$$\left.\begin{array}{l} \text{with } \phi_m = 2\ln\ (\frac{1+x}{2}) + \ln\ (\frac{1+x^2}{2}) - 2\tan^{-1} x + \frac{\pi}{2} \\ x \quad = (1-\alpha\ z/L)^{1/4} \end{array}\right\} z/L\ <\ 0 \tag{5.10}$$

$$\phi_m \quad = \beta_1\ z/L \qquad\qquad z/L\ >\ 0$$

These relations have been used to derive z_0, given the measured values of $\bar{u}$, u_* and L for each sensor.

5.4 "Mean" values

It was found that care was needed in calculating mean values, over all sensors in a particular trial, of quantities such as σ_u/u_*. If one sensor, as part of the statistical scatter, produces a particularly low value of u_*, this results in a large value for σ_u/u_*. When a mean of all the σ_u/u_* values is taken, this large value dominates the results.

Consequently, the "mean" value of σ_u/u_* used is the ratio of the mean σ_u to the mean u_*. (All means are weighted as described in Section 4.) A similar approach has been used for σ_w/u_*, σ_T/T_*, $1/L$ and μ. In each case means of the basic parameters were taken first, before combining them.

A similar problem occurs for the roughness length, z_0. The stability-corrected value of z_0 derived from one sensor may be strongly affected by the anomalous value for $\overline{w'T'}$ measured by that sensor. Thus, in deriving the "mean" z_0, roughness lengths have been calculated from each sensor using the "mean" $1/L$ in eqn. (5.9). A weighted geometric mean (arithmetic mean of

*Recent careful experiments of Högström [6] and Purtell et al. [29] which put the value of the von Karman constant k_v in the range 0.40 to 0.41, appear to support this analysis.

ln (z_0)) of the resulting values was then taken. This procedure removes the undue influence of single anomalous $\overline{w'T'}$ measurements.

6. Findings from sonic anemometer data

The results of the analysis can now be viewed as a whole. In this section we shall first examine some basic turbulence statistics for consistency with other experiments in the atmospheric boundary layer; this will be followed by an examination of the data on roughness length and atmospheric stability from the various Thorney Island Phase I trials. Note that in Figs. 4–13 and 15 the letters A–J are used to indicate trials 10–19 respectively.

For the characterisation of overall atmospheric stability during each of the trials, the "mean" value of 1/L, as discussed in Section 5, is an appropriate parameter. However, for an assessment of the dependence of turbulence statistics such as velocity fluctuations and correlation coefficients on stability, the dimensionless parameter z/L should clearly be used, in accordance with Monin–Obukhov similarity theory. Then the observations from individual sensors have to be plotted, rather than an average for each trial, since the sensor heights, z, vary.

6.1 σ_u/u_*, σ_w/u_*

Hicks [21] has presented the stability dependencies of various turbulence statistics for the Kansas data. σ_u/u_* has a level value of about 3 in strong instability, dropping to a neutral value $(z/L=0)$ of about 2.5, and decreasing further to below 2.2 in strongly stable conditions.* Ariel and Nadezhina [22] averaging results from twelve papers, find a neutral value of 2.4. For the Thorney Island data (Fig. 4), the strongly unstable values are widely scattered. However, the mean value near neutral $(|z/L|<0.1)$ is 2.37, and the one good stable trial, number 12, shows the continuing decrease of σ_u/u_* with increasing z/L.**

The measurements of σ_w/u_* show a clear dependence on z/L (Fig. 5). The near-neutral mean value is 1.34, which is consistent with the statement of Wyngaard et al. [23]: "There is consistent experimental evidence that $\overline{w'^2}^{1/2}/u_* \simeq 1.25 \pm 0.05$ at neutral". The unstable values are higher than the curve (due to Panofsky et al. [24]) found by Hicks [21] to fit the Kansas date:

---

*Note that u here refers strictly to the longitudinal component of velocity, whereas our values use the total horizontal component.

**Hicks [21] points out that plotting the data as in Fig. 4 introduces the possibility of spurious correlations since some of the same measurements are used in both ordinate and abscissa. However, our main purpose here is to show the measured σ_u/u_*, for example, are consistent with other observations.

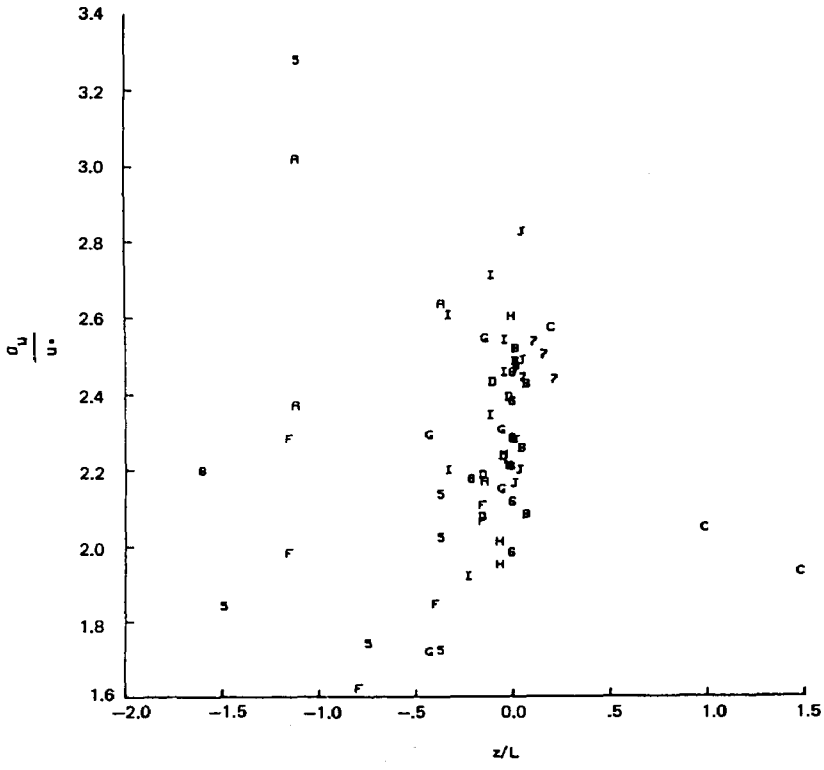

Fig. 4. Stability dependence of σ_u/u_*.

$$\sigma_w/u = 1.25\ (1-2\,z/L)^{1/3} \tag{6.1}$$

To avoid a singularity in σ_T/T_* at $z/L=0$, the measurement of σ_T/T_* have been plotted, following Ariel and Nadezhina [22], as $-(z/L)\ (\sigma_T/T_*)^2$ versus z/L (Fig.6). Ariel and Nadezhina find this parameter roughly constant at about 1.3 in unstable conditions, sharply decreasing to zero at neutral, with a continuing rapid decrease for further increase of z/L.* Figure 6 is roughly consistent with this, although there is large scatter on the unstable side, and only one data point significantly away from neutral on the stable side.

6.2 Velocity correlation coefficients

The correlation coefficient for momentum transfer can be defined as:

*Allowance has been made here for their slightly different definition of T_*, which includes the von Karman constant.

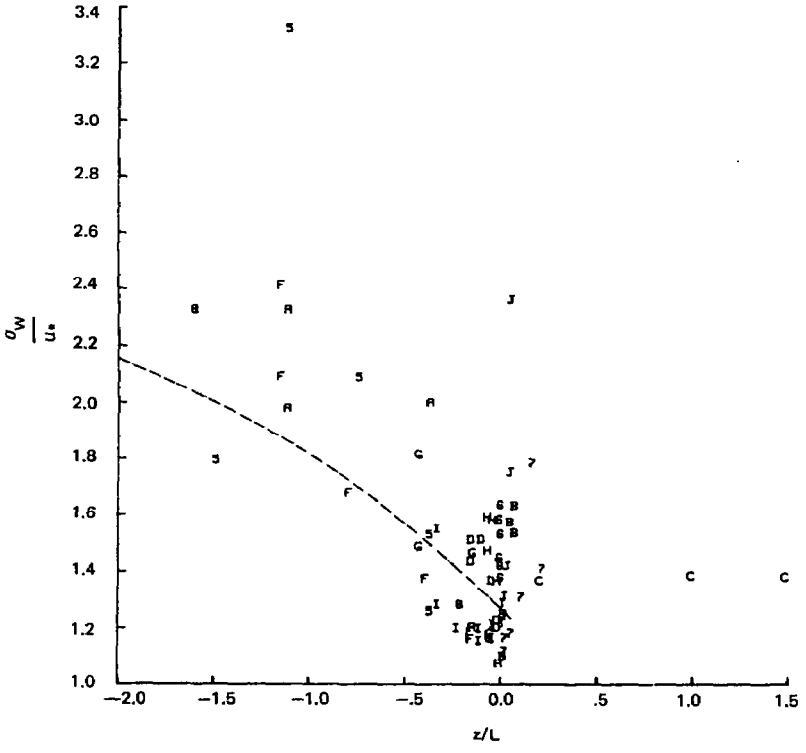

Fig. 5. Stability dependence of σ_w/u_*. The unstable values are generally higher than the prediction of eqn. (6.1) (dashed line).

$$r_{uw} = \frac{\overline{u'w'}}{\sigma_u \sigma_w} = -\left(\frac{\sigma_u}{u_*} \cdot \frac{\sigma_w}{u_*}\right)^{-1}$$

and for heat transfer:

$$r_{wT} = \frac{\overline{w'T'}}{\sigma_w \sigma_T} = -\left(\frac{\sigma_w}{u_*} \cdot \frac{\sigma_T}{T_*}\right)^{-1}$$

These coefficients measure the efficiency of the transport of momentum and heat by fluctuations in vertical velocity.

The Thorney Island measurements of r_{uw} are plotted in Fig. 7. The average value near neutral is 0.32. These observations are consistent with findings of Wesely [25] of 0.32 at neutral, decreasing to below 0.2 in strongly unstable conditions, and with the Kansas data [26] of 0.31 at neutral, decreasing to 0.14 for $-2 < z/L < -1$. Garrett [27] summarising results from several authors, has also noted a decrease from about 0.3 at neutral towards 0.1 in strong instability, provided the wind speed is not above 5 m/s.

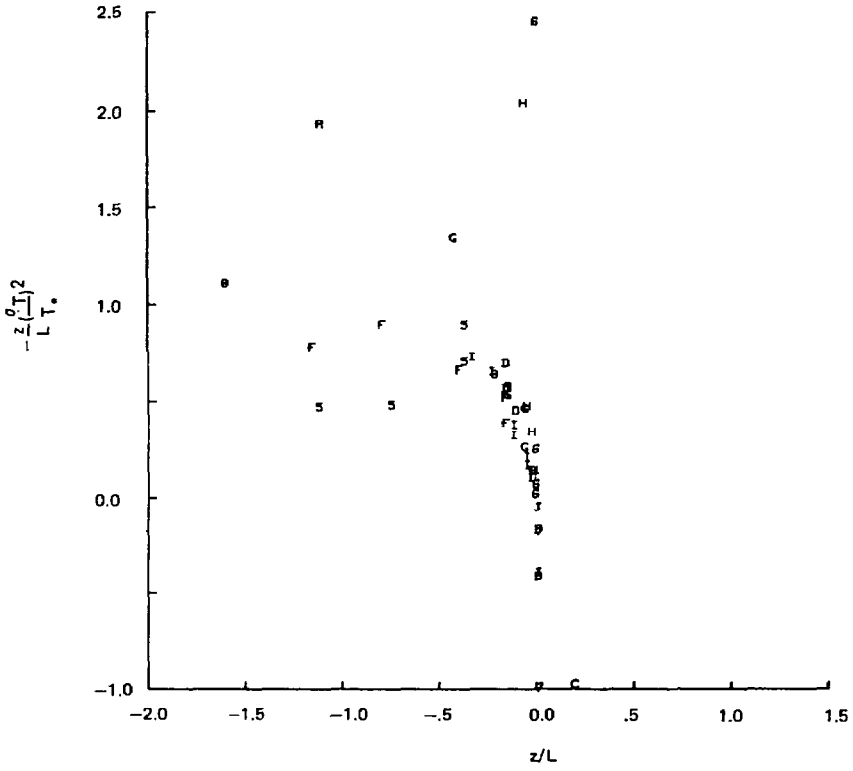

Fig. 6. $-z/L\ (\sigma_T/T_*)^2$ plotted against the stability parameter z/L. Several outlying points are outside the area of this plot.

In Fig. 8 r_{wT} is plotted. Garratt's sources find values between 0.45 and 0.6 in unstable conditions; the Kansas data give a mean value of 0.59 for $-2 < z/L < -1$. Figure 8 is consistent with these observations.

These findings principally provide reassurance that, in a number of basic measures, the turbulence data gathered at Thorney Island are consistent with previous atmospheric boundary layer measurements.

6.3 Roughness length

When the values determined for the roughness length z_0 for the fifteen trials are compared, it is found that they range over more than an order of magnitide, from 1.4 mm to 29 mm. This scatter is greater than would be expected, even allowing for the logarithmic nature of this parameter. There is no definite correlation with stability (Fig. 9), although the lowest values are found in unstable conditions. Equally, differences in wind speed do not appear to explain the range of values (Fig. 10). There is perhaps a tendency for lower values at

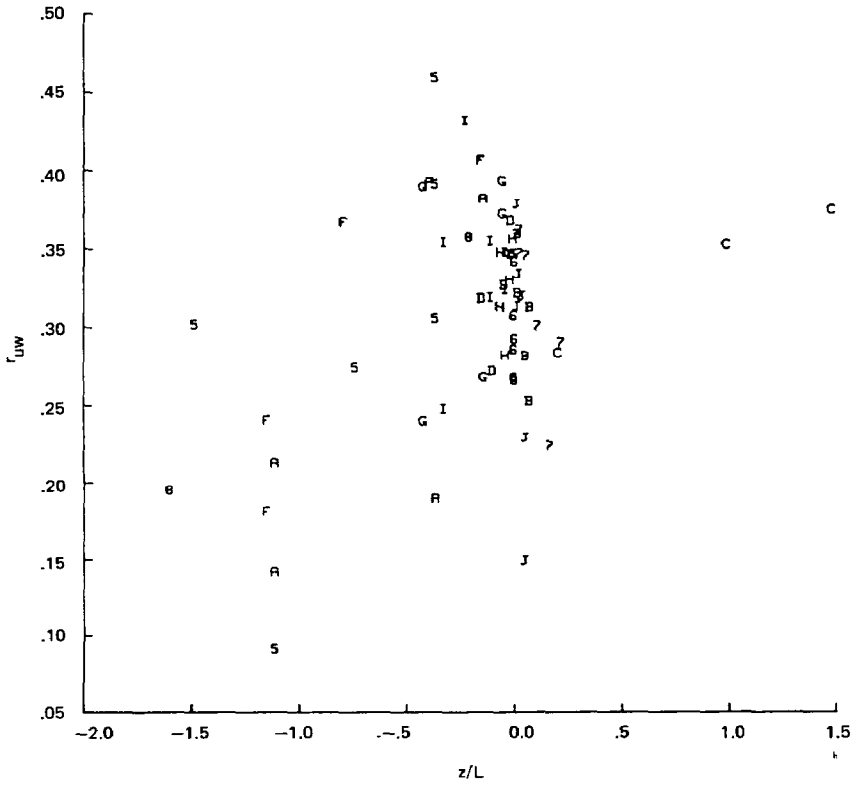

Fig. 7. Stability dependence of the correlation coefficient for vertical momentum transfer r_{uw}.

higher wind speeds, as has been noted before [3], but a definite effect cannot be deduced from these data.

Most informative is a plot of z_0 against wind direction (Fig. 11). This shows that the lowest values of z_0 are obtained for wind directions close to the axis of the sensor array, with a general increase in z_0 with deviation from the axis. In Fig. 12, where z_0 is plotted against the deviation of the wind direction from the axis, this is perhaps more clear. The data indicate a roughness of about 2–3 mm near the axis, climbing to about 18 mm for $\bar{\theta} \geqslant 50°$.

This variation with wind direction ought no to be unexpected since for off-axis winds there was a variety of obstructions upwind in the shape of trees and buildings, whereas close to the axis the wind was coming off the sea over flat grass. In fact, the spill point and sensor array were designed to give the greatest possible range of wind directions without obstructions upwind or downwind. It was intended that releases would only be performed for $\bar{\theta} \leqslant 31°$, and known that ideal upwind conditions only applied for $\bar{\theta} \leqslant 20°$. However, it was not always possible in practice to keep even within the $\pm 30°$ range.

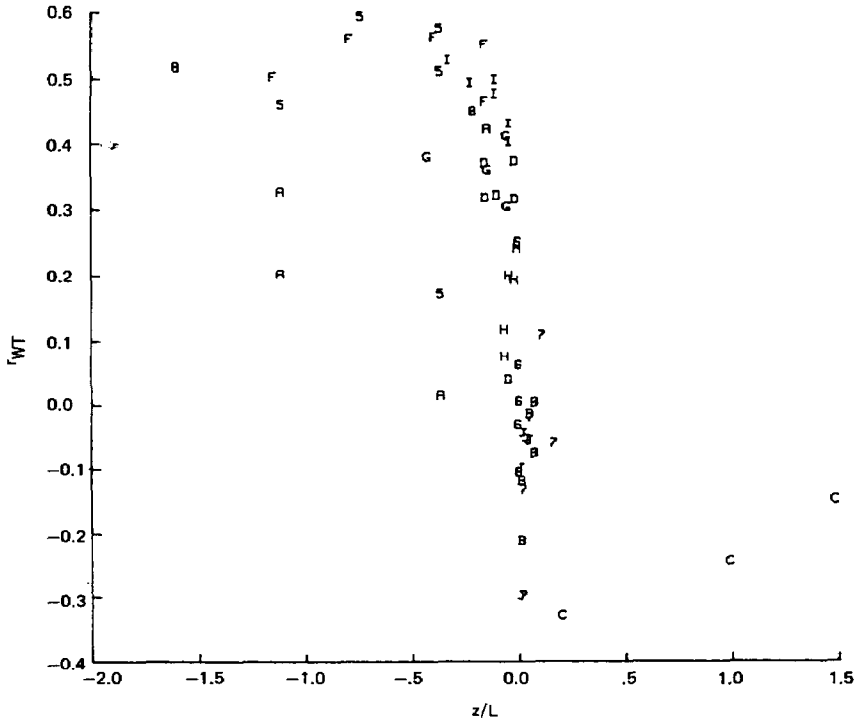

Fig. 8. Stability dependence of the correlation coefficient for vertical heat transfer, r_{wT}.

Given the closeness of the upstream obstacles for the off-axis winds, it might be thought that in these cases the boundary layer has not fully adjusted to the change of roughness, whereas for winds on the axis the upwind terrain was uniform. However, for such a grass surface Ref. [28] suggests a roughness of about 10 mm. The figure 2–3 mm found on the axis is closer to 1 mm for "off-sea wind in coastal areas". Thus in both cases the boundary layer was adjusting after a change in surface roughness. The measurements of Raabe [29] with some extrapolation, and those analysed by Wood [30] suggest an internal boundary layer depth at the measurement array of the order of 10 m in both cases.

It therefore seems likely that both for $\bar{\theta} \simeq 0$ and for $\bar{\theta} > 50°$ the boundary layer was in the late stages of adjustment to a surface rougness change, and that a fetch over several kilometers of grass would have given a roughness length about midway between the extremes of 2 mm and 18 mm.

6.4 Atmospheric stability

It is desirable to relate the values of the Monin–Obukhov length, L, and the Kazanski–Monin stability parameter μ derived here to Pasquill stability classes. Some dense gas dispersion models require the Pasquill class as an input param-

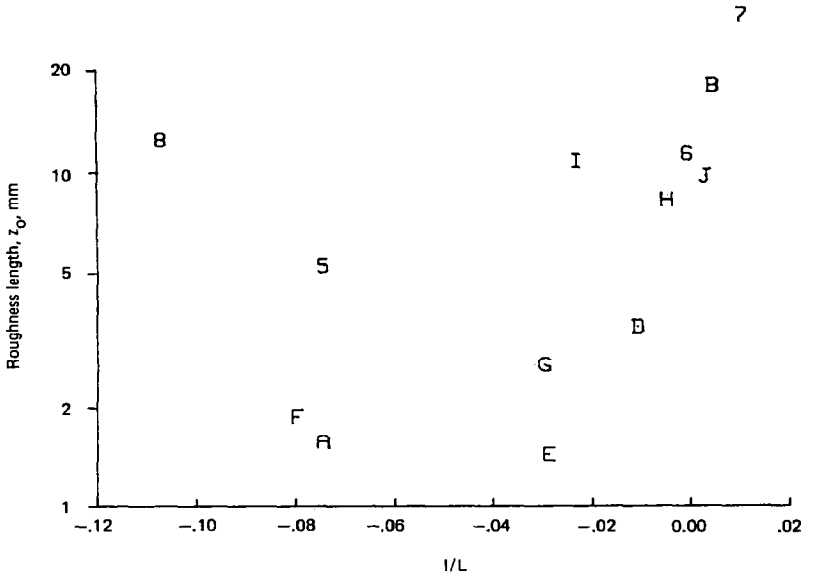

Fig. 9. The roughness length measured for each trial, plotted against the stability parameter $1/L$.

eter rather than the basic quantities. It is also interesting to relate these findings to the stability classes estimated from other observations [1,13].

Golder [32] has derived empirical relations between L and the Pasquill sta-

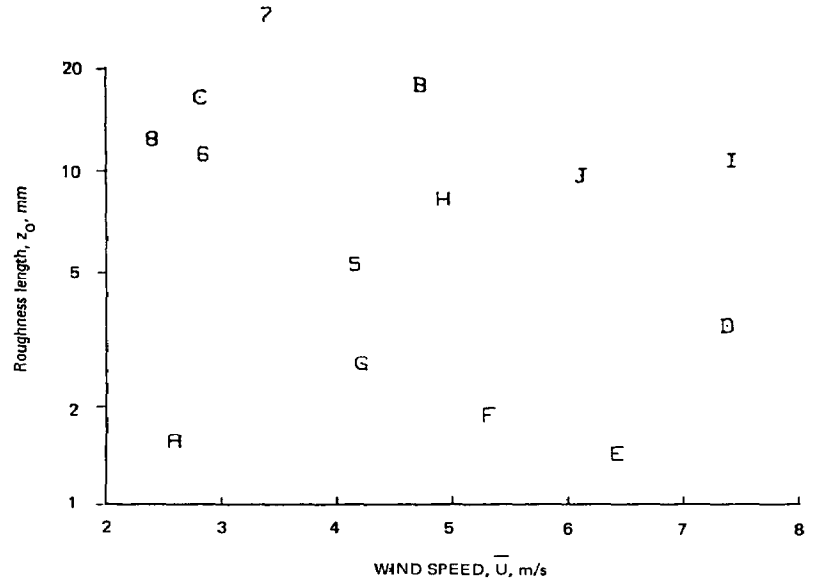

Fig. 10. Roughness length plotted against wind speed.

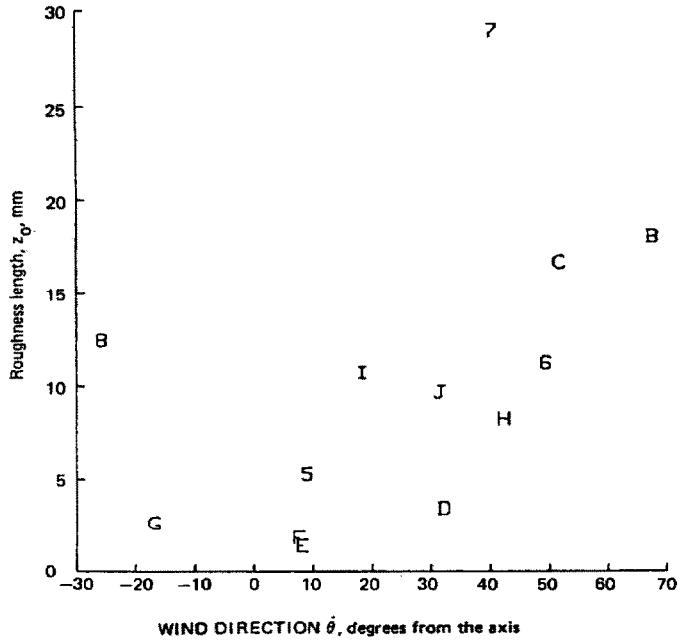

Fig. 11. Roughness length plotted against wind direction.

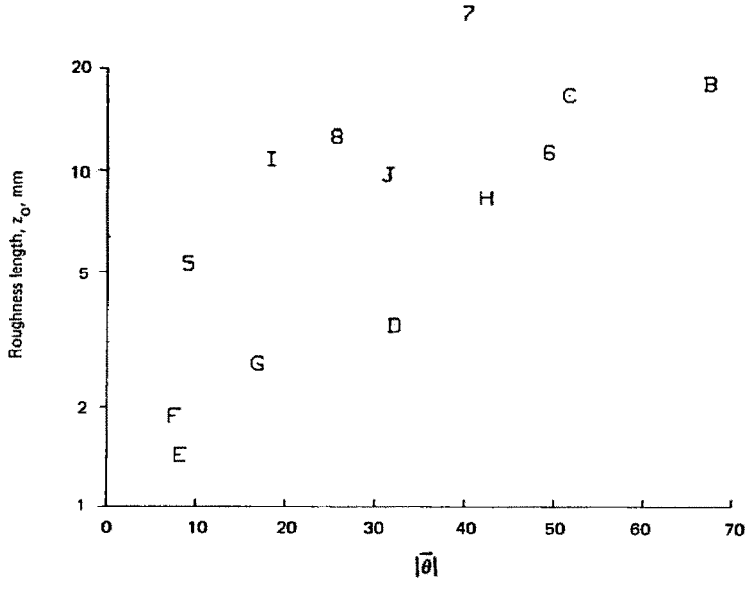

Fig. 12. Roughness length plotted against the deviation of the wind direction from the axis.

TABLE 2

Pasquill stability classes derived from the flux data, compared with the assignments originally made from other observations

Trial	From other data and observations (in data book [30])	From $1/L$ (Ref. [31])	From μ (Ref. [16])
5	B	B/C	B/C
6	D/E	D	D
7	E	D/E	D/E
8	D	B	B/C
9	F	F	F
10	C	C	C/D
11	D	D	D
12	E	F	F
13	D	D	D
14	C/D	D	D
15	C/D	B/C	B
16	D	C/D	C/D
17	D/E	D	D
18	D	C/D	C/D
19	D/E	D	D

bility classes, and Tagliazucca and Nanni [17] have done the same for μ. In both cases, the Pasquill class is a function both of L (or μ) and roughness length.

Using these references, and allowing for the variation of surface roughness with wind direction (Fig. 11), we obtain the results listed in Table 2. Given the large variation often found in various estimates of stability class, the agreement is very good. In only one trial (8) is there a change of more than one class. Individual trials are discussed in Section 10.

6.5 Thermometer corrections

Before looking at the data on temperature profiles from the meteorological mast, we should check whether there are consistent errors in the readings of the thermometers. These platinum resistance devices have a claimed accuracy of only 0.3°C, although their consistency from trial to trial is likely to have been considerably better than this. Temperature differences of under 0.1°C can be significant for the vertical separations of ~ 10 m. Davies and Singh [1] have noted anomalies in the measured temperature profiles.

Ideally, we should like to find data taken in a perfectly neutral atmosphere, where we would known that the actual potential temperatures would be the same at all levels, and the readings from the thermometers would show any offset present. The ideal neutrally-stable atmosphere is, however, rare. But we

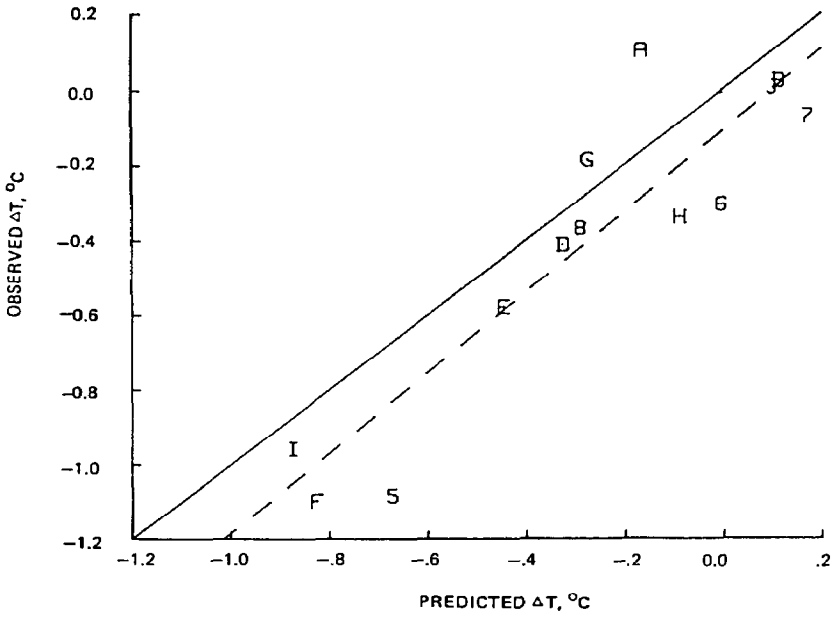

Fig. 13. Temperature differences between 9 m and 2 m, observed and predicted.

can use all the data we have, in various stabilities, and interpolate to neutral conditions.

Figure 13 shows the results of comparing observed potential temperature differences with those which are predicted by eqn. (5.3) using the measured heat flux.* The dashed line gives a linear regression fit to the data. The gradient is close to one.

Using the dashed line in Fig. 13 and similar plots for other heights to interpolate to neutral, the necessary corrections are found to be $+0.11°$ at 9 m, $-0.06°$ at 16 m, $+0.06°$ at 22 m and $+0.11°$ at 30 m.

7. Velocity and temperature profile data

7.1 Velocity profiles

The velocity profile data for several trials are plotted in Fig. 14. The raw data are plotted as small circles, and the results of multiplying by 0.94 to allow for anemometer overspeeding (see Section 2.2) are plotted as crosses. For each trial a simple logarithmic fit to the whole profile has been made:

$$\bar{u}\,(z) = \frac{u_*}{0.41} \ln \frac{z}{z_0} \tag{7.1}$$

*See the discussion of temperature profiles in Section 7.2.

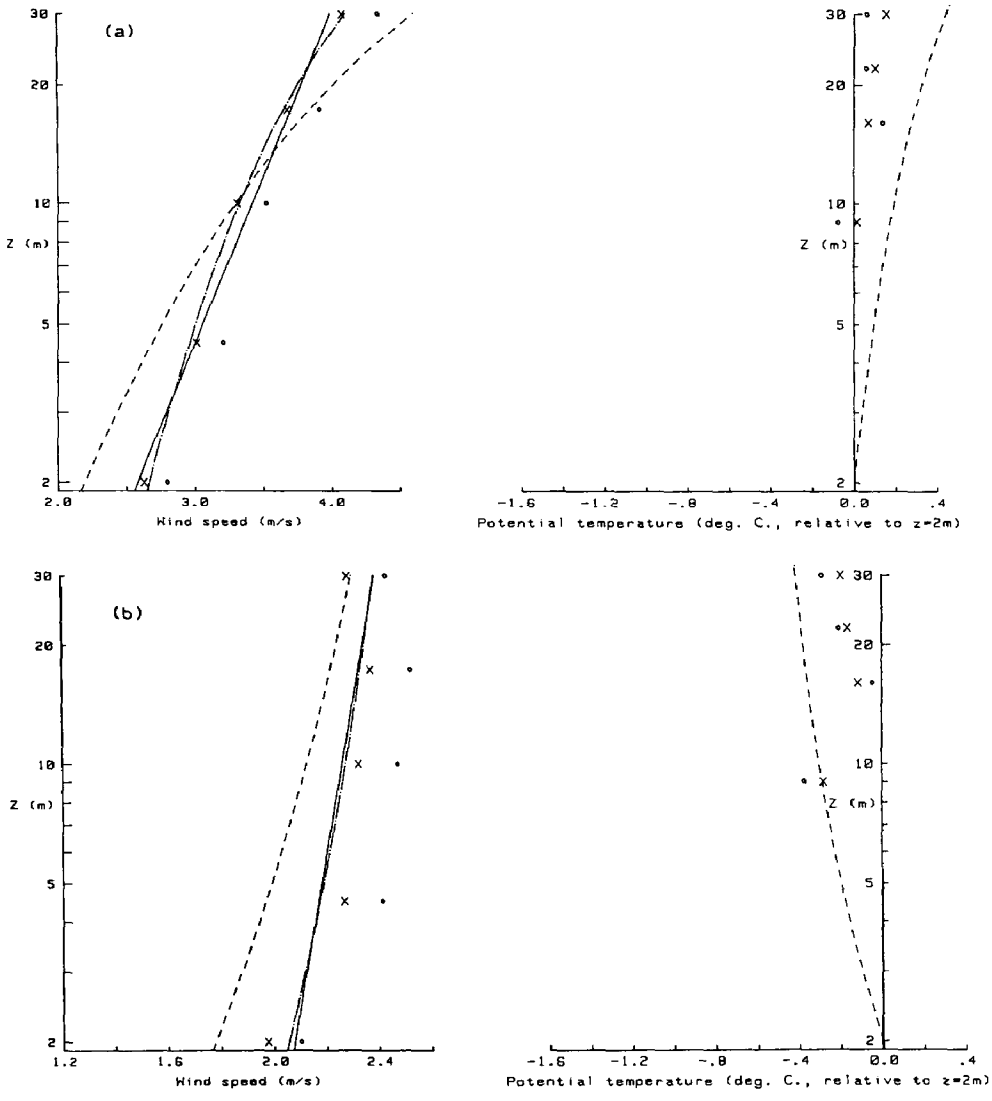

Fig. 14. Velocity and temperature profiles. o raw data; × corrected data; (———) logarithmic profile fit (eqn. 7.1); (–·–·–) profile fit allowing for stability (eqn. 5.9 with L determined from fluxes); (- - -) profile predicted from flux data: (a) Trial 7, (b) Trial 8.

This is plotted as a continuous line. To allow for stability, a further curve fit was made using eqn. (5.9) taking L as derived from the flux measurements.

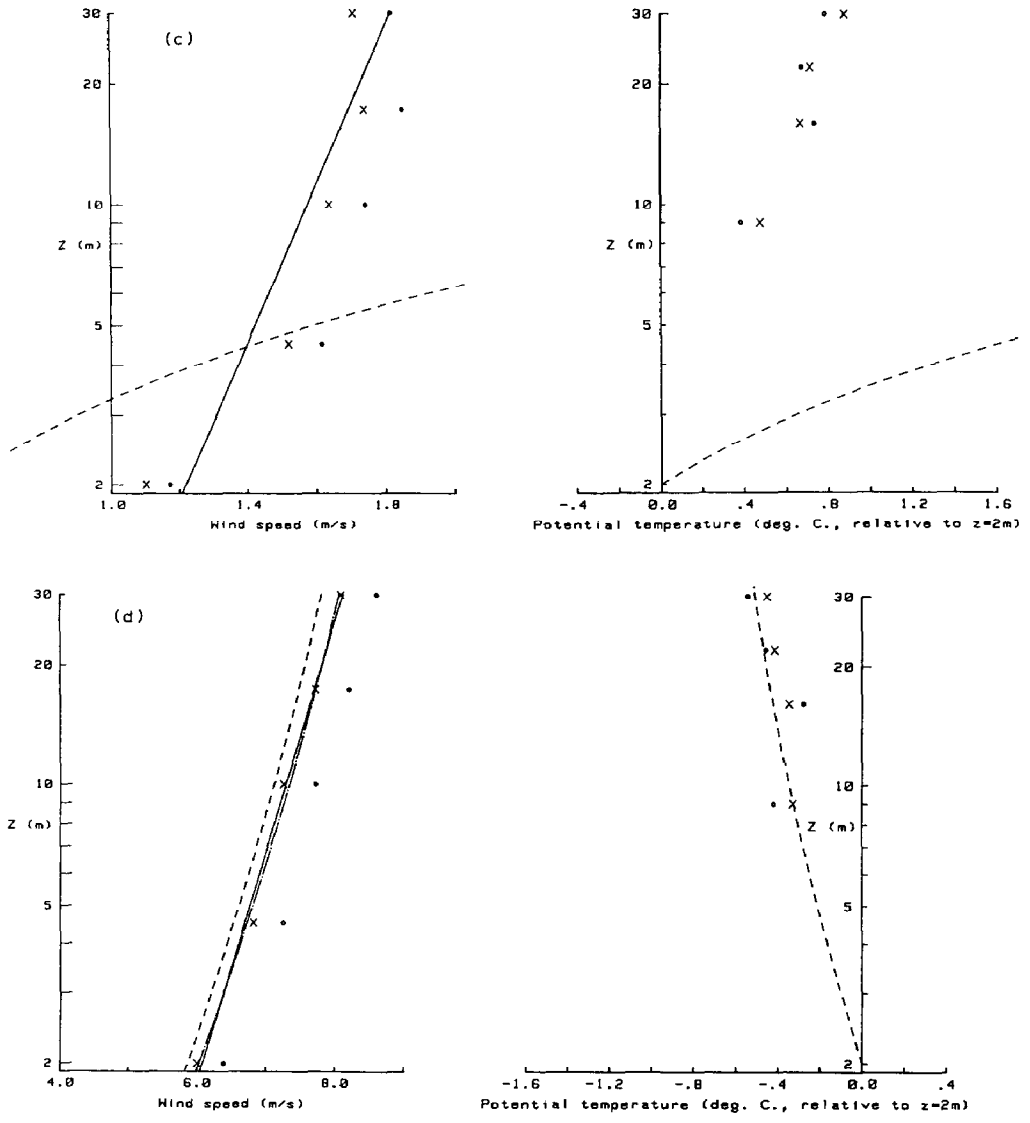

Fig. 14 (continued). (c) Trial 9, (d) Trial 13.

Each fitted curve gives estimates for u_* and z_0.* These z_0 are plotted against θ in Fig. 15.

In almost every case the observed velocity difference between the bottom

*It would have been possible to estimate u_*, z_0 and L entirely from the velocity and temperature profile data by the non-linear fitting procedures of Nieuwstadt [33] but we have not attempted this. It appears unlikely that it would be worthwhile for these profile data.

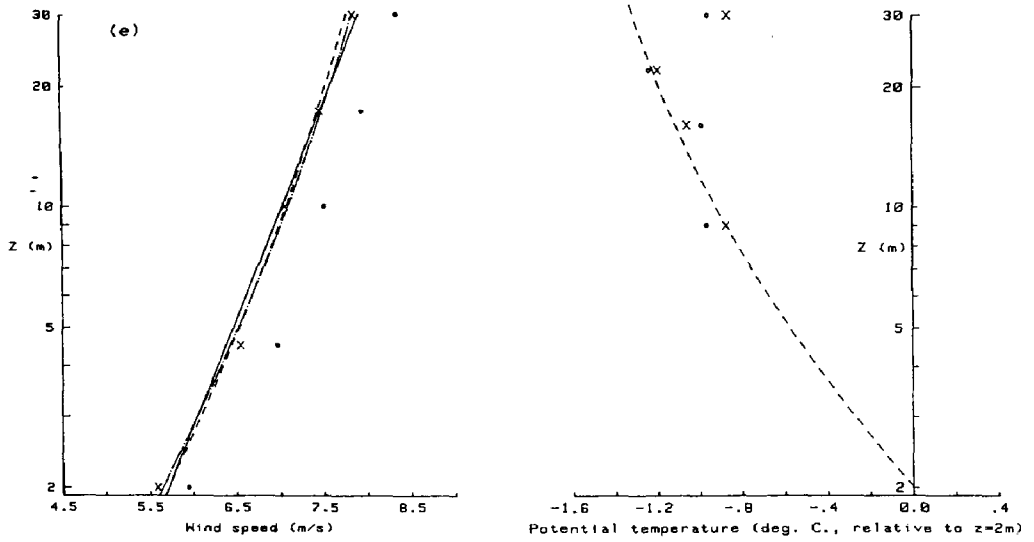

Fig. 14 (continued). (e) Trial 18.

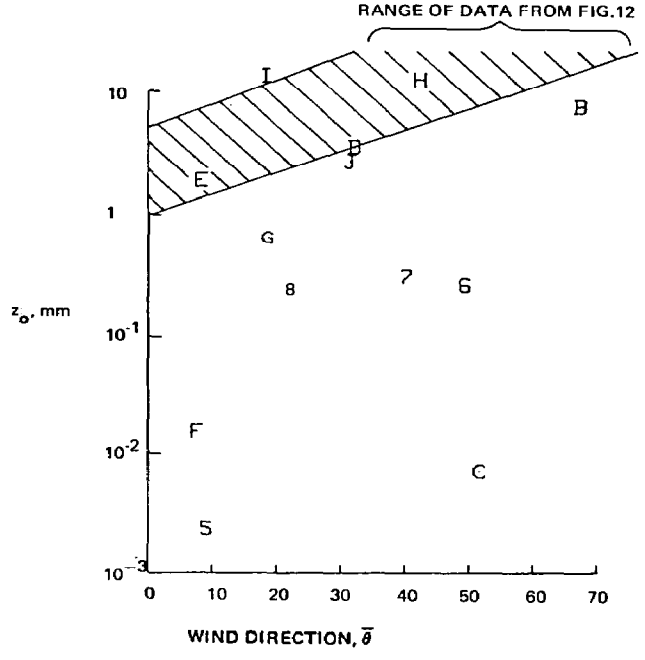

Fig. 15. Roughness length obtained by curve-fitting velocity profiles, with allowance for stability.

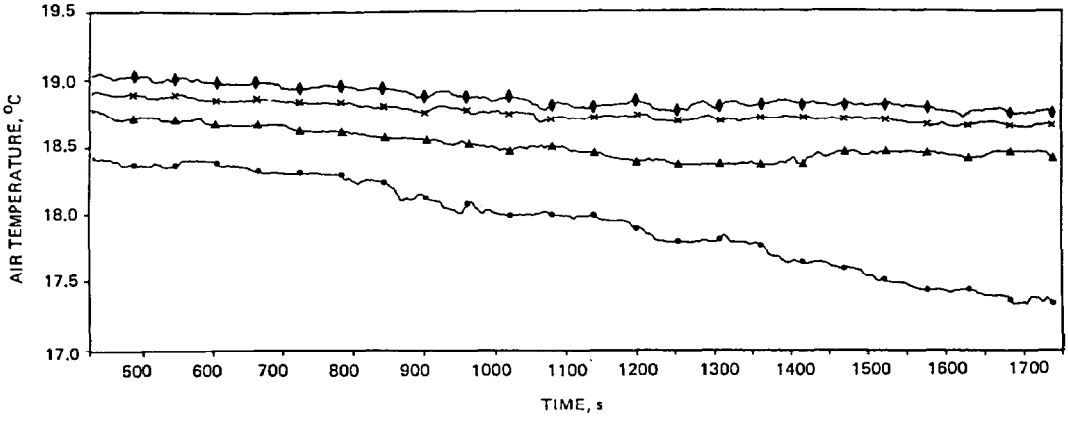

Fig. 16. The development of the temperature profile during Trial 9 at heights -●- 2 m, -▲- 9 m, -✳- 16 m, and -◆- 22 m.

two sensors (at 2 m and 4.5 m) is greater than in the fitted curve. This is consistent with the generally low values of z_0 obtained by this method, (Fig. 15) compared with the flux data which are biassed towards the lowest few metres of the boundary layer. The generally poor fit of the profiles is reflected in the very large scatter of estimates in Fig. 15.

The velocity profiles inferred by inserting the flux-derived values of u_*, L and z_0 into eqn. (5.9) are plotted in Fig. 14 as dashed lines.

7.2 The temperature profiles

Temperature profiles obtained from the meteorological mast are also plotted in Fig. 14. Again raw data are shown as small circles and the corrected values (Section 6.5) as crosses. The temperature profile deduced from the flux measurements, using eqn. (5.3), is plotted in the figures as a dashed line.

The agreement between these predicted profiles and the measurements is generally very good, as in the two neutral trials, 13 and 18, plotted. The largest discrepancies appear to occur when the stability in the lowest part of the boundary layer, where the flux measurements were concentrated, does not continue up to 30 m. This occurs particularly in the two strongly stable cases, 9 and 12, and in the unstable Trial 8. The good agreement adds confidence to the assessments of atmospheric stability based on the flux measurements (Section 6.4).

8. Comments in individual trials

From the analysis reported in the last two sections, the following observations about individual trials can be made. For a full description of the mete-

orological circumstances surrounding each trial, these comments should be read in conjunction with the "History" section of the relevant data book [31].

8.1 Trial 5

This trial shows a particularly poor fit of the profile data, and unusually large variability in the shear-stress ($\overline{u'w'}$) measurements. These might be associated with the rapidly changing conditions in the early stages of sea-breeze development.

8.2 Trial 6

Trial 6 was performed in the early evening following a day of moderate insolation. Thus conditions were moving from unstable towards stable. The upper part of the temperature profile still shows the unstable gradient, but the lower part is consistent with the neutral stability obtained from the heat flux measurement.

8.3 Trial 7

Performed at the same time of evening as Trial 6, but following a day with less sun, Trial 7 shows a very consistent, slightly stable, temperature profile (Fig. 14a). The mean flux measurement indicates a little greater stability, giving a Pasquill category of D/E. This mean value is influenced by values of downward heat flux at 2 m which were larger than those measured higher up. It is likely that a more stable layer was beginning to grow but reaching no more than 2 or 3 m from the surface at this time, so not affecting the measured temperature profile.

8.4 Trial 8

This was one trial where there was a significant difference between the estimated stability and that derived from the flux measurements. The instability found may be due to a sea-land temperature difference, since this is one of only three trials where the wind was coming from the direction of the open sea. The profile data (Fig. 14b) show a temperature difference consistent with the flux measurements between 9 m and 2 m, followed by an inversion between 9 m and 16 m.

8.5 Trial 9

Trial 9 (Fig. 14c) was remarkable for the observations of very long persistence of the gas near the ground following the spill. The evidence points to the existence of a developing shallow strongly-stable layer close the ground. At the start of data collection, this layer was less than 2 m thick, and the temperature measured at 2 m remained fairly constant (Fig. 16). After 13 minutes, the temperature at 2 m started to drop, which can be interpreted as the top of the layer reaching this level then and continuing to grow.

In such circumstances, the flow above the layer can become almost decoupled from the ground, as evidenced by the shear stress dropping almost to zero, and the visual observations of very low wind speed in the lowest metre.

The assignment of F stability to this trial appears appropriate to the region of the boundary layer in which the gas was dispersing.

In view of the apparent extreme departure in this case from constant-flux conditions, data from Trial 9 have generally been excluded from averages in this paper.

8.6 Trial 10

The wind direction in Trial 10 was exceptional, being more than 90° from the spill axis. The thermal conditions, while less extreme, were probably the reverse of those in Trial 9. Stable stratification had developed during the night. After an hour and half of morning sun, a shallow convective layer would explain the positive vertical heat flux measurements.

8.7 Trial 11

This trial, performed in the late afternoon of a day with low insolation, shows excellent agreement between temperature profile and flux measurements — very slightly stable but remaining within the D category.

8.8 Trial 12

Trial 12, like Trial 9 but less extreme, shows a developing stable layer beneath a neutral profile. The resulting shear-stress measurements give a wide scatter of estimates of u_*. The flux-derived temperature profile is probably good for about the first four metres, but is too steep above that.

8.9 Trial 13

Trial 13, like Trial 11, was performed in near-neutral conditions (this time slightly unstable) well away from the changes of morning or evening, resulting in an excellent temperature profile fit (Fig. 14d) and very consistent shear-stress measurements.

8.10 Trial 14

Trial 14, the last of 1982, was performed in similar conditions to Trial 13 at midday in late October. The atmosphere was slightly more unstable. Good agreement for the temperature profile was again found. The wind speed was low, around 3 m/s, until 280 s after the start of data collection; at this time, 40 s before the release of the bag, it suddenly increased to about 6 m/s and remained steady. To avoid this discontinuity only data collected after 290 s has been used in the analysis. Since in this trial data collection was stopped after only 630 s, the remaining usable data period is 220 s, after allowing for the run-up and run

down of the moving-average filter. As a result the consistency of the shear-stress measurements is poorer than usual.

8.11 Trial 15

Performed in the mid-afternoon of a sunny day in late April, Trial 15 provides the best-defined unstable conditions of the series. Generally the temperature profile is in good agreement with the flux measurements.

8.12 Trial 16

Trial 16 was performed three hours after Trial 15, by which time the insolation was very low (170 W/m^2), so that only slightly unstable conditions prevailed. A temperature inversion at the upper levels is surprising, but it may be due to the wind's now coming from an offshore direction as in Trial 8.

8.13 Trial 17

Trial 17, performed just before 8 p.m. in early June, provides the most consistent set of shear-stress measurements of the whole series, individual u_*-estimates varying from 0.26 to 0.31 m/s. This consistency is probably due to the low insolation during the day, giving near-neutral stability. The temperature profile is, unaccountably, slightly ragged.

8.14 Trial 18

In low insolation, in the mid afternoon of a day which had been sunny earlier, the atmosphere here still shows signs of moderate instability — Pasquill category C/D. The $\overline{w'T'}$ measurements were notable in this case by their consistency, and show good agreement, up to 22 m, with the temperature profile measurements (Fig. 14e).

8.15 Trial 19

Five hours later on the same day as Trial 18, the atmosphere had become very slightly stable but still well within the Pasquill "D" category. Flux-derived predictions and measurements of the temperature profile were again in close agreement up to 22 m.

9. Conclusions

1. The input parameters atmospheric stability and surface roughness have been derived for the Thorney Island Phase I trials principally from the analysis of data from ten sonic anemometers to determine vertical momentum and heat fluxes. Long averaging times, or the data from many sensors, are necessary in such analysis in order to obtain good estimates of the mean values of the quantities of interest.

2. Careful examination of sonic anemometer signals is necessary to eliminate error from a variety of faults.

3. Corrections of sonic-anemometer data for tilt and flow distortion, and for errors caused by non-alignment with the wind direction appear satisfactory.

4. In all but four trials, use of high-pass filtering with a moving average period of 120 s leads to reduced standard errors.

5. The effective surface roughness is about 2–3 mm for wind directions close to the axis of the measuring array. But as the wind direction moves away from the axis, the roughness increases, reaching about 18 mm for wind directions more than 50° from the axis. It appears that, at both extremes, the boundary layer was in the late stages of adjustment to a change in surface roughness. For winds near the axis, the flow was off the sea or sand; away from the axis there were trees and buildings upwind. A fetch of several kilometers over grass would probably give a surface roughness about midway between the extremes.

6. The atmospheric stability categories obtained from the heat flux measurements are generally in good agreement with those already deduced from careful assessment of other data. The one marked difference involves an occasion when a shallow convective layer was starting to grow near the surface, giving an unstable atmosphere in the bottom few metres; this trial was previously categorised as neutral.

7. Examination of the velocity and temperature profiles provides a more complete picture of the meteorological conditions during each trial, especially on those occasions where the near-surface conditions contrasted with those higher up. The velocity profile does not give good estimates of the surface roughness, probably owing to the upstream changes in roughness. After correction, the temperature profiles are generally in very good agreement with predictions from the flux data.

References

1 M.E. Davies and S. Singh, Thorney Island: its geography and meteorology, J. Hazardous Materials, 11 (1985) 91–124.

2 J.S. Puttock, Comparison of Thorney Island data with predictions of HEGABOX/HEGADAS, J. Hazardous Materials, 16 (1987) 439–455.

3 D.R. Johnson, Thorney Island trials: systems development and operational procedures, J. Hazardous Materials, 11 (1985) 35–64.

4 J.S. Puttock and G.W. Colenbrander, Thorney Island data and dispersion modelling, J. Hazardous Materials, 11 (1985) 381–397.

5 J.C. Wyngaard, Cup, propellor, vane and sonic anemometers in turbulence research, Ann. Rev. Fluid Mech., 13 (1981) 399–423.

6 U. Högström, Von Karman's constant in atmospheric boundary layer flow: re-evaluated, J. Atmos. Sci., 42 (1985) 263–270.

7 A.J. Dyer, Flow distortion by supporting structures, Boundary Layer Meteorol., 20 (1981) 243–251.

8 J.C. Wyngaard, Comments on "Flow distortion by supporting structures", Boundary-Layer Meteorol., 22 (1982) 263–268.

9 A.J. Dyer, Reply, Boundary-Layer Meteorol., 22 (1982) 267–268.

10 P. Schotanus, F.T.M. Nieuwstadt and H.A.R. de Bruin, Temperature measurements with a sonic anemometer and its application to heat and moisture fluxes, Boundary-Layer Meteorol., 26 (1983) 81–93.

11 J.C. Kaimal, J.C. Wyngaard and D.A. Haugen, Deriving power spectra from a three-component sonic anemometer, J. Appl. Meteorol., 7 (1968) 827–837.

12 G.A. McBean and J.A. Elliott, The vertical transports of kinetic energy by turbulence and pressure in a boundary layer, J. Atmos. Sci., 32 (1975) 753–766.

13 L. van Haren, Direct measurements of momentum and buoyancy fluxes at Maplin Sands, Private communication, 1984.

14 G.A. McBean, The turbulent transfer mechanisms: a time domain analysis. Q. J. R. Meteorol. Soc., 100 (1974) 53–66.

15 A.S. Monin and A.M. Yaglon, Statistical Fluid Mechanics, Volume I, MIT Press, Cambridge, MA, 1971.

16 F.B. Smith, The relation between Pasquill stability P and Kazanski–Monin stability μ (in neutral and unstable conditions), Atmos. Environ., 13 (1979) 879–881.

17 M. Tagliazucca and T. Nanni, An atmopheric diffusion classification scheme based on the Kazanski–Monin stability parameter, Atmos. Environ., 17 (1983) 2205–2211.

18 A.K. Lo and G.A. McBean, On the relative errors in methods of flux calculations, J. Appl. Meteorol., 17 (1978) 1704–1711.

19 J. Wieringa, A re-evaluation of the Kansas mast influence on measurements of stress and cup anemometer overspeeding, Boundary-Layer Meteorol., 18 (1980) 411–430.

20 L.P. Purtell, P.S. Klebanoff and F.J. Buckley, Turbulent boundary layer at low Reynolds number, Phys. Fluids, 24 (1981) 802–811.

21 B.B. Hicks, An examination of turbulence statistics in the surface boundary layer, Boundary-Layer Meteorol., 21 (1981) 389–402.

22 N.Z. Ariel and Ye.D. Nadezhina, Dimensionless turbulence characteristics under various stratification conditions, Izv. Acad. Sci.,USSR, Atmos. Oceanic Phys., 12 (1976) 802-809 (492–497 in translation).

23 J.C. Wyngaard, J.A. Businger, J.C. Kaimal and S.E. Larsen, Comments on "A re-evaluation of the Kansas mast influence on measurements of stress and cup anemometer overspeeding", Boundary-Layer Meteorol., 22 (1982) 245–250.

24 H.A. Panofsky, H. Tennekes, D.H. Lenschow and J.C. Wyngaard, The characteristics of turbulent velocity components in the surface layer under convective conditions, Boundary-Layer Meteorol., 11 (1977) 355–361.

25 M.L. Wesely, Magnitudes of turbulent fluctuations in the atmospheric surface layer, In: Proc. Symposium on Atmospheric Diffusion and Air Pollution, Santa Barbara, CA, American Meteorology Society, Boston, 1974, pp. 15–18.

26 J.C. Kaimal, J.C. Wyngaard, Y. Yzumi and O.R. Coté, Spectral characteristics of surface-layer turbulence, Q. J. R. Meteorol. Soc., 98 (1972) 563–589.

27 J.R. Garratt, Limitations of the Monin–Obukhov similarity theory for turbulent transfer of momentum in unstable conditions in the atmospheric surface layer, Q. J. R. Meteorol. Soc., 101 (1975) 169–172.

28 ESDU Data Sheet 74031, Characteristics of atmospheric turbulence near the ground — Part II, Single point data for strong winds (neutral atmosphere), Engineering Sciences Data Unit, London, 1974.

29 A. Raabe, On the relation between the drag coefficient and fetch above the sea in the case of off-shore wind in the near-shore zone. Z. Meteorol., 33 (1983) 363–367.

30 D.H. Wood, Internal boundary layer growth following a step change in surface roughness, Boundary Layer Meteorol., 22 (1982) 241–244.
31 Health and Safety Executive, Heavy gas dispersion trials, Thorney Island 1982-3, data for Trials 5–19 (fifteen reports) HSE, Sheffield, Great Britain.
32 D. Golder, Relations among stability parameters in the surface layer, Boundary-Layer Meteorol., 3 (1972) 47–58.
33 F. Nieuwstadt, The computation of friction velocity u_* and the temperature scale T_* from temperature and wind velocity profiles by least-square methods, Boundary-Layer Meteorol., 14 (1978) 235–246.